ChemElectroChem

Research Article
doi.org/10.1002/celc.202300532

Chemistry Europe
European Chemical Societies Publishing

www.chemelectrochem.org

An Autonomous Electrochemical Discovery Robot that Utilises Probabilistic Algorithms: Probing the Redox Behaviour of Inorganic Materials

Kristine Laws[+],[a] Marcus Tze-Kiat Ng[+],[a] Abhishek Sharma,[a] Yibin Jiang,[a] Alexander J. S. Hammer,[a] and Leroy Cronin*[a]

The discovery of new electroactive materials is slow due to the large combinatorial chemical space of possible experiments. Efficient exploration of redox-active chemical space requires a machine learning assisted robotic platform with real-time feedback. Here, we developed a closed-loop robotic platform which is capable of synthesis and electrochemical characterisation controlled using a probabilistic algorithm. This was used to probe the redox behaviour of different polyoxometalates (POMs) precursors and explore the formation of redox-active coordination complexes. The system can run accurate analytical electrochemical measurements whilst maintaining the performance and accuracy of both the working and reference electrodes. The platform successfully ran and analysed 336 coordination chemistry reactions by performing *ca.* 2500 cyclic voltammetry (CV) scans for analysis and electrode cleaning. Overall, the platform carried out over 9900 operations in 350 hours at a rate of 28 operations per hour, and we identified 24 complex solutions which showed significantly different redox activity. Experiments were performed using a universal chemical synthesis language (χDL) with variable inputs. The platform was used autonomously to investigate a range of POM precursor materials demonstrating 45 % increase in capacitance. The experiments ran for 36 hours with more than 6400 operations during which we analysed 200 POM precursor solutions.

Introduction

Understanding electrochemical processes is vital for the development of new devices for use in energy,[1,2] materials,[3–5] and biochemical research, as well as for probing the fundamentals of chemical bonding, structure, and reactivity.[6–8] Due to the large variables which can be investigated for the research areas mentioned previously, an automated analysis system could significantly improve the efficiency of the investigations. Using a more selective process to streamline the discovery of useful compounds can be achieved by implementing machine learning. Most of the research which has coupled machine learning and electrochemistry has focused on the analysis of cyclic voltammetry (CV) and stochastic amperometric data, or electrochemical simulations.[9–13] Whilst this shortens the time frame for understanding the electrochemical response from the compounds under investigation, we reasoned that combining this with automation would accelerate the discovery process. In the last five years, several strategies have used machine learning on robotic platforms to discover and optimise more efficient electrolytes for lithium batteries.[14] However, this approach has been limited and is rarely employed for the synthesis of chemical compounds. Different automation strategies have been adopted such as batch,[15] continuous flow reactors,[16] and integrated workstations for the exploration and optimisation of different chemistries.[17,18] While there has been significant research in automated synthesis,[15,16,18–20] this has mainly focused on organic reactions and has yet to be paired with electrochemistry.

The current research paradigm focuses on the automation of the synthetic route, execution of chemical synthesis, and the use of machine learning (ML) to accelerate the discovery of new reactions.[21,22] Combining these automated systems with electrochemistry is hindered due to the necessity of sustaining standards required when carrying out analytical electrochemistry. Electrochemistry requires regular cleaning of the electrode surface, which is commonly undertaken by manual polishing or electrochemical cleaning.[23,24] Additionally, monitoring the condition of the reference electrode is necessary to ensure there is no contamination, which could lead to drifting electrochemical measurements and inaccurate results.

Supramolecular structures such as Polyoxometalate clusters (POMs) have shown promising results in catalysis and energy storage materials owing to their diverse, tunable bulk electronic properties.[22,25,26] However, the mechanism of the relationship between the ions and the self-assembly process is still under investigation. In addition, highly soluble redox-active inorganic

[a] *Dr. K. Laws,[+] Dr. M. Tze-Kiat Ng,[+] Dr. A. Sharma, Dr. Y. Jiang, Dr. A. J. S. Hammer, Prof. Dr. L. Cronin*
School of Chemistry
University of Glasgow
Glasgow, G12 8QQ (UK)
E-mail: lee.cronin@glasgow.ac.uk

[+] *These authors contributed equally to this work.*

Supporting information for this article is available on the WWW under https://doi.org/10.1002/celc.202300532

complexes which are heavily utilised in energy storage and CO_2 recapture as well as biological and medicinal active agents[27] were also a selected investigation. Exploring a high-dimensional chemical space using electrochemical signatures as a measure of uniqueness would provide an opportunity to understand how supramolecular compounds form and discover new complexes. This exploration is best achieved using a combinatorial high throughput approach, achieved with a closed-loop system to provide real-time analysis of the electrochemical performance, which can then provide the next set of reaction conditions with the highest probability for improvement.

Here we present an electrochemical autonomous redox utility system, 'ECARUS', a robotic platform with the capability to synthesise a variety of inorganic compounds and characterise their electrochemical behaviour for new material discovery (Scheme 1). ECARUS was constructed of 2 modules (Figure S1–3, Table S1); a chemical module (Figure S4–12) which could execute up to 24 reactions in parallel and fine-tune the solution pH. The second module is electrochemical (Figure S13–14), which allows the study of the electrochemical properties of redox-active complexes and electrolytes.

Furthermore, the system is designed to be autonomous with the capability of optimising electrochemical behaviour on the fly (Figure S15–17). The platform was able to complete 480 synthetic protocols and analyse the products in 385 hours. The combination of automation with parallel synthesis means that each experiment takes on average 48 minutes and saves the chemist over one and a half months of manual hours, before considering the improved efficiency of robotic handling, control, and automated cleaning.

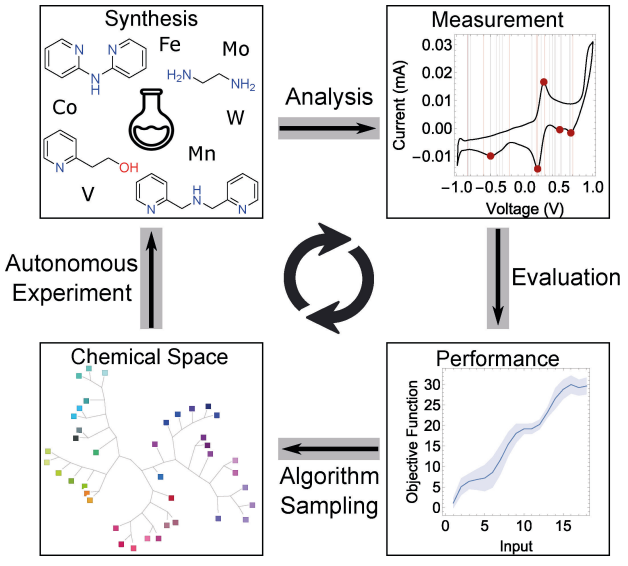

Scheme 1. Schematic workflow of ECARUS. The self-driving workflow combines robotic experiments and machine learning to optimise the redox properties of electrolytes and complexes, associating a digital signature to each experiment to ensure reproducibility and standardisation of procedure between batches.

ECARUS Workflow

The general protocol for ECARUS consists of 4 main procedures: 1) synthesis via liquid dispensing of stock solutions and pH control, 2) CV measurement, followed by essential cleaning of the electrodes after each sample, 3) reactor cleaning in preparation for the next experiment, 4) data analysis and information extraction for machine learning algorithms which suggest further investigation. The experimental platform and repetition synthesis and analysis cycle are shown in Figure 1. Full details outlining the platform hardware and software can be found in the SI in sections 1 and 2, respectively. The platform is run using a software system based on the open-source universal chemical programming language standard, χDL; an example of the analysis and cleaning cycle χDL for one sample can be seen in Figure 1c. As a result of the adaptability of χDL, all experiments were run using 3 sets of χDL files which executed over 16,300 operations in total to complete the experiments discussed below.

The chemistry selected for exploration here was based on electrochemically active metals, with the aim of synthesising a variety of inorganic compounds, from simple coordination complexes to larger supramolecular structures such as polyoxometalates. The platform forms complexes by selecting from a maximum of four possible ligands combining with two metal salts or solely investigating the combinations of three metal oxide salts, thus demonstrating the robust and versatile chemistry the platform can perform. These synthesis inputs were selected to provide a high-dimensional chemical space to explore.[28–32]

The electrode holder was designed to hold three electrodes in the middle of reactor vials without being in contact with each other. The holder was mounted on an XZ motor to move the electrodes between the sample to analyse on the chemical reaction module or the cleaning station and lower the electrodes into the sample or cleaning/storage solutions. It is necessary to clean the surface of the working electrode between each sample measurement, electrochemical cleaning of the working electrode is more reliably implemented on a robotic platform rather than the typical polishing by hand, but this requires regular standard CVs to be run ensuring the precision of the electrodes.

Following the sample measurement of the metal complex solution, Figure 2a shows an example CV, the electrodes are moved to the cleaning station of the platform to undergo electrochemical cleaning, rinsing and storage in KCl. Cleaning of the working electrode gold surface is achieved by running multiple CV scans in sulphuric acid (0.1 M) between −0.5 V and 1.5 V at a scan rate of 100 mV s^{-1}. As the working electrode is thoroughly cleaned after each sample measurement, 5 scans in sulphuric acid were used for each cleaning cycle, this is to ensure the gold electrode is not degraded by frequent contact with strong acid. Following this, the electrodes are rinsed with aqueous KCl solution and finally stored in KCl solution (3 M), necessary to protect the reference electrode, until required again. The recorded CVs of the cleaning cycles are used to

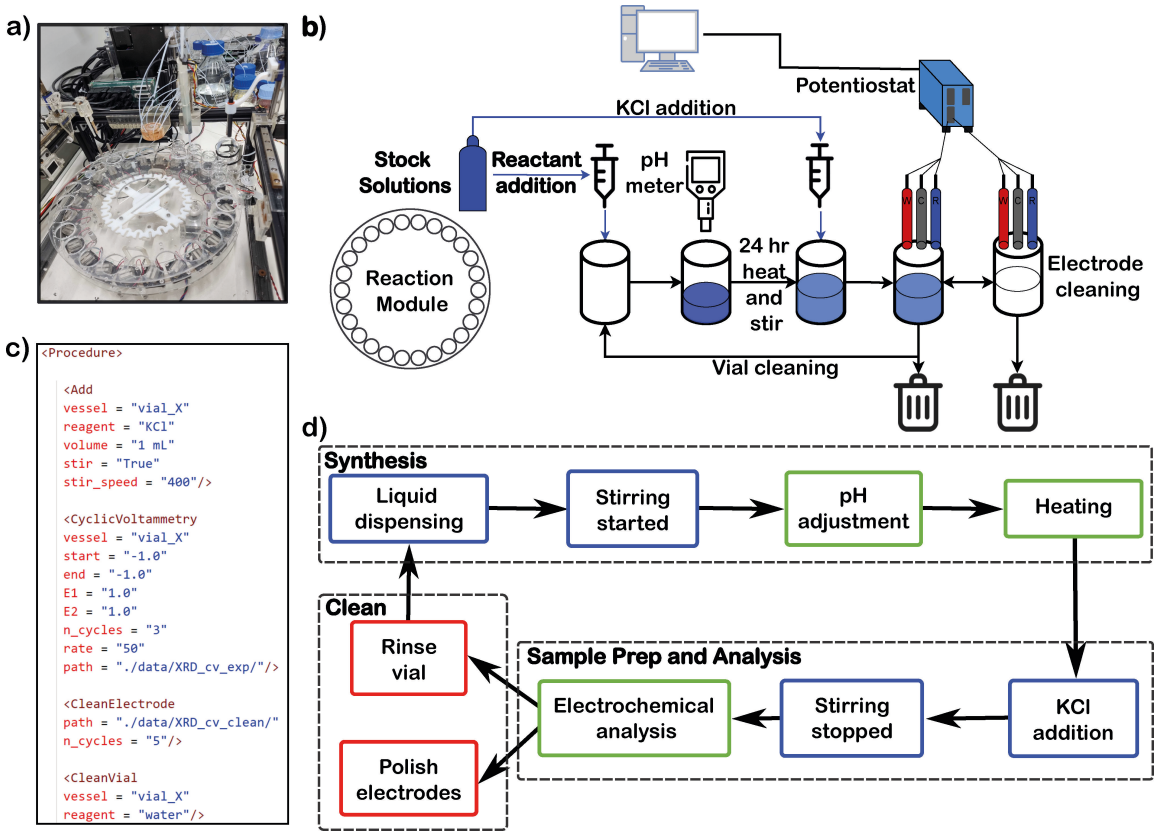

Figure 1. Components in the ECARUS self-driving platform. (a) Picture of the robotic platform (ECARUS), (b) Representation of the platform; highlighting the main components required for each step, (c) XDL procedure for running the electrochemical analysis (d) general synthetic protocol used by ECARUS, outlining the 3 main physical steps performed by the platform.

check the condition of the working and reference electrodes by comparing the CVs as each cleaning cycle progresses.

To ensure the platform produces reproducible and reliable data it was essential to dispense and analyse a known concentration of a well characterised redox couple in solution. Therefore, potassium ferricyanide/ferrocyanide ($K_3/K_4[Fe(CN)_6]$, 0.05 M, with 0.1 M KCl supporting electrolyte), was used to test the measurement and cleaning cycle for the electrode module, Figure 2b shows 22 example CVs collected during the test run. The oxidation and reduction peaks of the $[Fe(CN)_6]^{3-/4-}$ redox couple are highlighted. Analysis of the peak position shows the average of the oxidation peak is $+0.293 \pm 0.003$ V and the reduction peak is -0.181 ± 0.004 V. The redox peak position had small standard deviations for both redox peaks which is indicative of a well-maintained reference electrode and no drifting of voltages can be seen. The average current for the redox event was calculated as $+0.141 \pm 0.007$ mA and $+0.133 \pm 0.006$ mA for the oxidation and reduction peaks respectively, which shows the reliability of the working electrode as the standard deviation for the tests is minimal, as well as the consistent dispensing by the material across 22 reaction vials.

Importantly the working electrode must be clean before being used for the analysis, Figure 2c shows an example H_2SO_4 cleaning cycle which was collected during the $K_3/K_4[Fe(CN)_6]$ tests, as $[Fe(CN)_6]^{3-/4-}$ is known to foul gold. The CV highlights the characteristic gold oxide peak, which can be seen to quickly converge at $+0.858$ V with a standard deviation of ± 0.008 V, showing that the working electrode is effectively cleaned during the 5 scans. The $K_3/K_4[Fe(CN)_6]$ test CVs consistently show almost identical CVs signifying ECARUS to be capable of successfully simulating parallel synthesis and characterisation of compounds whilst maintaining clean and accurate electrodes.

Results

Synthetic coordination chemistry

Cobalt coordination chemistry is a field which continues to grow due to the relatively low cost and availability of the metal as well as its redox activity. It is an essential element for prokaryotes and plants as micronutrients and as the active centre in coenzymes such as B12 in mammals.[13] As such most research currently focuses on applications of cobalt complexes; with examples in medicinal chemistry as biomimetics and drug-like molecules. It has also found use as catalysts or energy storage, proving the versatility and importance of cobalt coordination chemistry which is still to be fully explored.[33]

Initially, ECARUS was used to synthesise cobalt complexes by simply combining $CoCl_2$ with up to four possible bidentate ligands; 2,2′-bipyridine (Ligand 1/L1), 4,4′-bipyridine (Ligand 2/

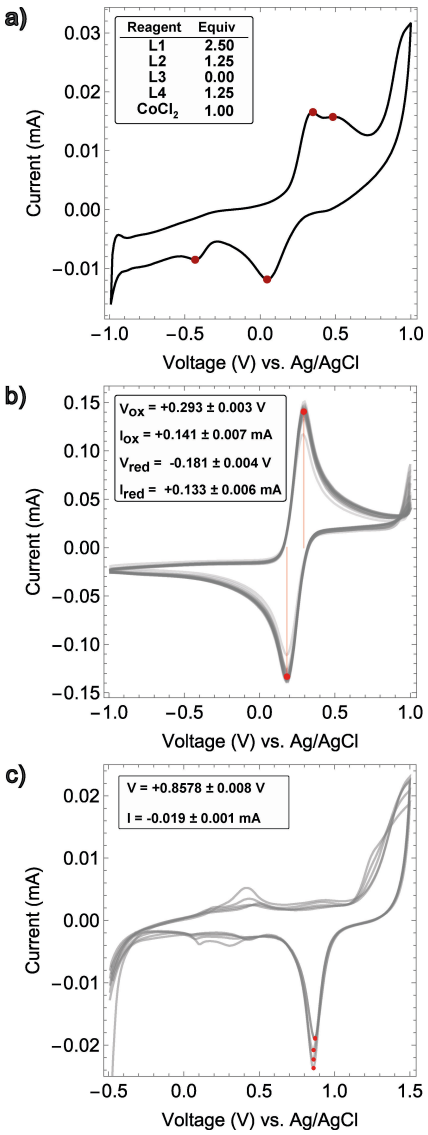

Figure 2. Graphs showing example CVs obtained by ECARUS, a) shows an example of a typical cyclic voltammogram obtained on the gold electrode during the grid search when combining $CoCl_2$ and the ligands with the equivalence shown in the table insert, b) cyclic voltammogram of ferricyanide/ferrocyanide solution (0.05 M total concentration, Au electrode, 10 $mV\,s^{-1}$), with the mean voltage and mean current of the redox peaks and standard deviation across 22 solutions dispensed and measured using ECRAUS, c) example cyclic voltammogram of the gold electrode in H_2SO_4 (5 scans) between −0.5 and 1.5 V vs. Ag/AgCl at a scan rate of 100 $mV\,s^{-1}$, scan was performed as a cleaning procedure after each sample. The characteristic gold oxide removal peak is highlighted and the mean voltage and current for the peak are noted along with the standard deviation across the scans.

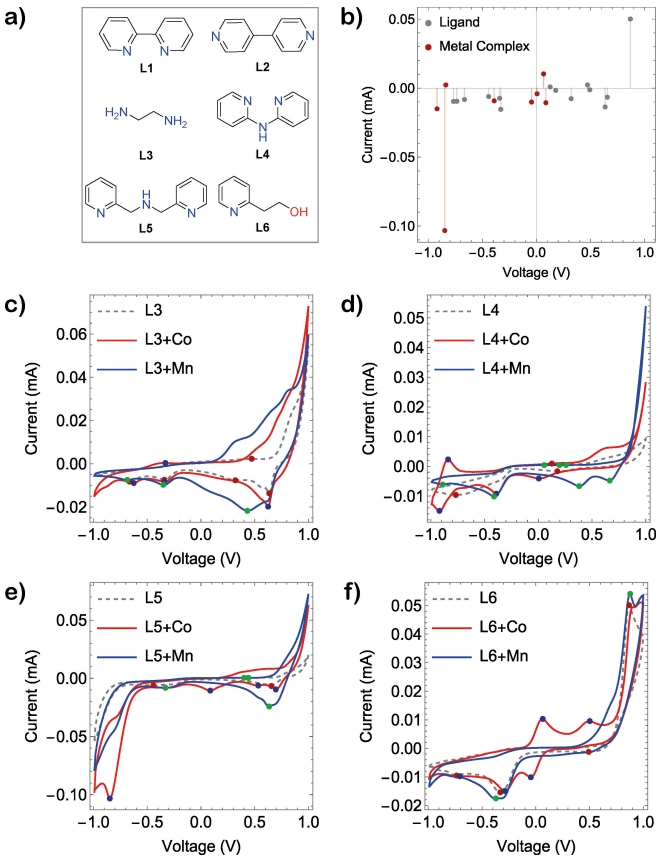

Figure 3. Graphs showing cobalt and manganese coordination chemistry control experiments run on ECARUS, a) the chemical structures of the ligands (L1–L6) used as 2 M and 1 M stock solutions, b) graph showing the peak position and intensity of CV peaks from control ligand and control metal complexes formed using a basic peak search routine, c–f) CVs of ligands 2–6 respectively, and the complexes formed from a 1 : 3 ratio of metal to ligand, these were used as controls.

L2), ethylenediamine (Ligand 3/L3) or 2,2′-dipyridylamine (Ligand 4/L4), see Figure 3a. The first set of experiments combined cobalt with 3 equivalences of each ligand individually to use as control experiments as these are well-known complexes, Table S2 and Figure S18.

Following the control experiments, a grid search was employed varying the combinations of ligands added and their equivalences. However, due to the presence of 2,2′-bipyridine (L1), which is a strong field ligand able to form stable complexes with the metal-ligand bond reinforced by the chelate effect, most of the CVs showed the presence of a strong redox event at 0.22 V. This voltage is consistent with a high concentration of cobalt tris-bipyridyl, showing a greater preference for the formation of $[Co(L1)_3]^{2+}$ over any other complexes. Therefore, to increase the diversity of the mixtures Ligand 1 and Ligand 2 were replaced by 2-pyridineethanol (Ligand 5/L5) and di-(2-picolyl)amine (Ligand 6/L6), as well as the addition of a manganese salt, ligand structures are shown in Figure 3a. Control CVs were obtained for the new chemical space, this included CVs of the ligands alone, and then the combination of each ligand (L3/L4/L5/L6) with each metal salt individually, with an equivalence of 3 : 1 ligand:metal (Figure 3c–f). Figure 3b shows the peak position and intensity of the redox peaks picked from each of the control CVs, with red dots representing peaks from metal complex CVs and grey dots representing ligand-only redox events. It is important to note that due to extreme diversity in the behaviour of peaks in CV, some peaks appearing like a plateau might be ignored.

A second grid search was employed to probe the chemical space and a larger variety of CV profiles were obtained (Figure S18). Analysis of the grid search CVs picked the peaks of significant redox events and overlaid the CV with the peak

positions of the control experiments from Figure 3b. Following this a selection of the CVs which have peaks at positions different to the controls or peaks which could indicate the presence of a novel redox couple were selected, the overlaid graphs of the selected CVs can be found in the SI Figure S19. Following this comparison process 24 CVs were selected as having redox peaks which could be of interest and their synthesis reactions were repeated and the samples subjected to further analysis, Figure S20. The samples were analysed by UV-Vis spectroscopy and compared to control UV-Vis spectra to check for the occurrence of any novel peaks. The UV-Vis spectra, which can be found in the supplementary information Figures S21–25, show that 8 of the 24 samples have UV-Vis peaks which are different from the controls and merit further investigation manually, more full analysis of the peaks and novelty of the spectra can be found in SI Section 3.5.

Role of acid in redox active electrolyte

Polyoxometalate (POM) chemistry is known to be pH sensitive therefore, to further understand how POMs form, a grid search was employed to investigate the extent of influence acid type and concentration can have. Sulphuric and phosphoric acid are regularly employed when synthesising POMs, therefore the experiments focused on exploring the effect of each acid separately on typical POM starting materials such as $Na_2MoO_4 \cdot 2H_2O$, $Na_2WO_4 \cdot 2H_2O$ and $NaVO_3$. Initially, the volume of each experiment was normalised to 10 mL with the metal salt volume set to a constant (4 mL, $Na_2MoO_4 \cdot 2H_2O$, $Na_2WO_4 \cdot 2H_2O$ (1.5 M), $NaVO_3$ (0.2 M)) for each experiment and remaining volume was varied between the selected acid (H_2SO_4 or H_3PO_4, 1.5 M) and DI water. Following the mixing of the reagents, the pH was measured and recorded and the CV was recorded between −1.2 to +1.0 V, Figure S26.

Figures 4a and 4b show the expected sigmoidal-shaped curves between the strong acid (H_2SO_4) and weak acid (H_3PO_4), all CVs for each metal salt in both acids can be found in the SI Figure S26. Each of the metal salts in the aqueous solution showed different inherent buffering capacity towards each of the acids at different concentrations.[34,35] In the case of tungstate species, however, precipitation was observed below pH 2.0. The formation of the precipitate observed likely originates from the low solubility of tungstic acid at lower pH.[36] Molybdate species conversely redissolve by coordinating with water molecules, forming dimeric complexes and becoming the building blocks for the formation of POMs.[37,38] A volcano relationship between the cathodic peak current and pH was observed for all the metal salts in H_2SO_4, which suggests that the reduction process is more favourable in that given range of pH, Figure S27–29. The cathodic peak current of Mo species in H_2SO_4 peaked around pH 0.7, while the cathodic peak current of W species in H_2SO_4 peaked around pH 2.0. Interestingly, the apex of the cathodic peak currents is consistent with the desirable pH from the literature for POM formation (see SI section 3.7).

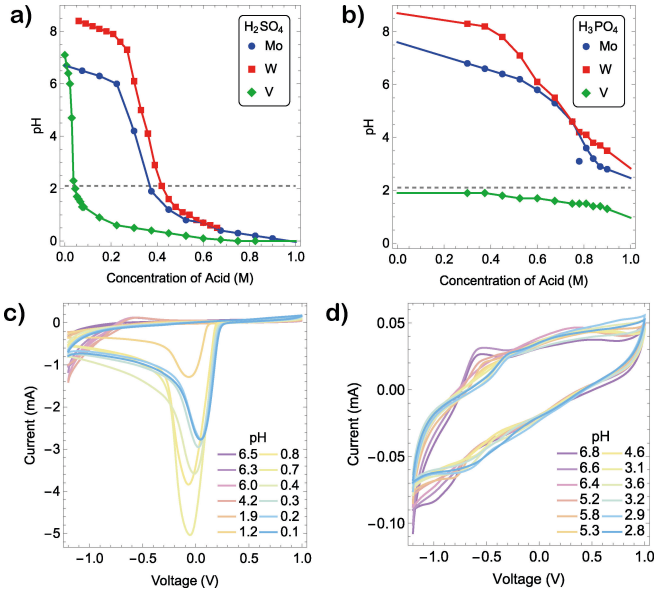

Figure 4. Investigation of the pH response of POM precursors with sulphuric or phosphoric acid, run using the platform. a) The pH response of the individual metal salts, Na_2MoO_4 (blue circle), Na_2WO_4 (red square) and $NaVO_3$ (green diamond) in different concentrations of sulphuric acid, b) The pH response of the individual metal salts, Na_2MoO_4 (blue circle), Na_2WO_4 (red square) and $NaVO_3$ (green diamond) in different concentrations of phosphoric acid. The CV of solutions of Na_2MoO_4 at pH values from 0.1–6.5 in H_2SO_4 (c) and from pH 6.8–2.8 in H_3PO_4 (d).

Autonomous optimisation of electrochemical behaviour

To achieve a closed-loop platform, a Bayesian optimisation algorithm was coupled with the robotic platform to navigate the available metal oxide chemical space, Figure S30. The 6-dimensional chemical space explored came from the following reagents: $Na_2MoO_4 \cdot 2H_2O$ (1.5 M), $Na_2WO_4 \cdot 2H_2O$ (1.5 M), H_2SO_4 (1.5 M), H_3PO_4 (1.5 M), Na_3VO_4 (0.74 M) and $Na_2S_2O_4$ (0.25 M). A single objective Bayesian optimisation algorithm was employed with the goal of maximising the CV area of the redox electrolyte. The objective of this approach is to demonstrate that the closed-loop approach is capable of top-down screening to navigate through a given chemical space for a specific goal. By using the workflow as shown in Scheme 1, ECARUS was able to navigate through the chemical space rapidly and the CV profile produced by the experiments quickly converged in the given chemical space to maximise the area. To initiate the closed-loop experiment, ten initial experiments were generated by the algorithm and carried out experimentally by the robotic platform, details of the reagents can be found in Table S4 and Figure S31-32. These initial experiments were used as training data in the Bayesian optimisation algorithm and the objective given to the algorithm was to minimize the negative of the CV area. In the following iterative experiments, a batch size of four was used based on the six continuous variables and experiments were carried out.

The convergence plot in Figure 5a showed that via the iterative closed-loop experiment, over time the Bayesian optimisation algorithm reached the minima of the objective

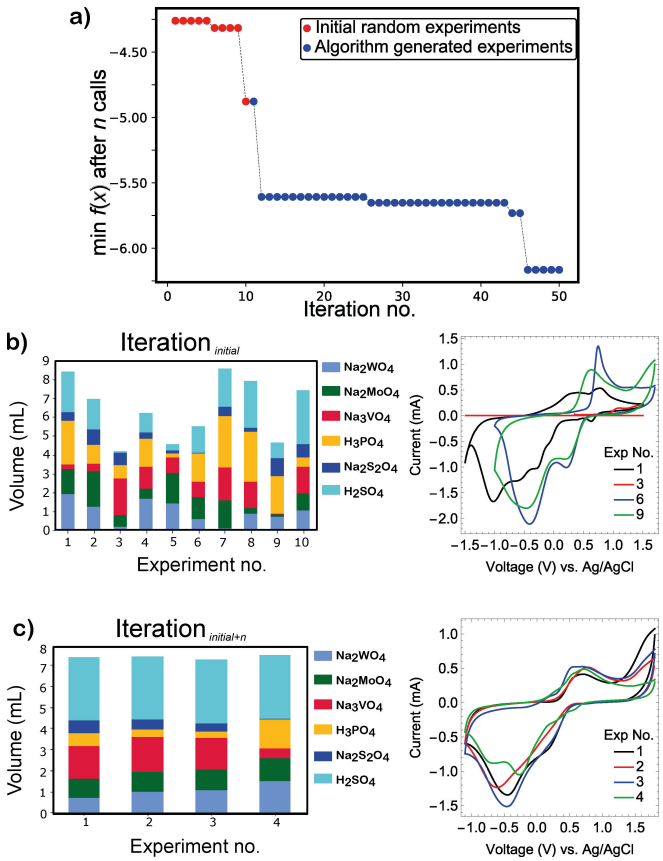

Figure 5. Iterative experiments with closed-loop optimisation. (a) Convergence plot highlighting the minimisation of the objective function over the experimental iterations, where f(*X*) is -CV area. (b) Volume dispensed of the reagents and a selection of the corresponding CV showing that the initial experiments possess diverse electrochemical behaviour, (c) reagent volume dispensed, and the corresponding CVs of experiments suggested by the algorithm which converge to similar electrochemical behaviour.

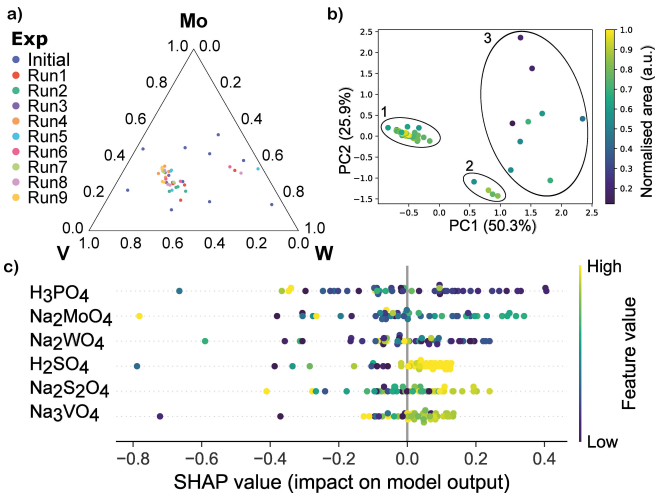

Figure 6. Space explored by ECARUS via closed-loop approach. (a) Normalised ternary plot of the metal salts between the initial random experiments (Initial) to the final experiments generated by optimisation algorithm (Run 9). (b) Two-component PCA analysis showing three distinct clusters, the scale of 0.0 (minimum) to 1.0 (maximum) was calculated from the normalised area of the CV. (c) SHAP summary plot of the reagents and the impact on the model output.

function (negatively related to the CV area), which was exhibited by the increased CV area overall and correlates to enhanced performance of the electroactive material. As seen in Figure 5, a noticeable contrast was observed when initial experimental CVs (Figure 5b) were compared with the CVs from experiments suggested by the optimisation algorithm (Figure 5c).The main difference is that the initial experiments provided a more diverse set of CV profiles, whereas the experiments suggested by the explorative algorithm had analogous CV profiles, and overall larger areas (Figure S33) Following this observation, a ternary plot of the three metal species was plotted and the coverage space of the experiments at different iterations were compared.

The initial iteration (Initial) depicted in Figure 6a was used to train the optimisation algorithm, while the following iterations were suggested by the algorithm and carried out by the robotic platform in an iterative process. Evidently, the experiments from the Initial provided a better coverage space and the following iterations clustered in a limited region with a few exceptions. To get a better understanding of the impact of the six continuous variables from all the experiments, principal component analysis (PCA) analysis was carried out. The separation of three distinct clusters was observed over the initial random experiments when compared to the experiments suggested by the algorithm with exploitation mode.

Based on the PCA as shown in Figure 6b, it was evident that PC1 and PC2 have a huge impact on the chemistry. Hence, the clustering of experiments was observed when the algorithm was in exploitative mode. Cluster 1 in Figure 6b was generated from the optimisation algorithm (exploration mode), while cluster 2 was generated from the optimisation algorithm as well and showed different CV profiles. The points observed in cluster 3 are the initial experiments carried out which showed a wider coverage compared to clusters 1 and 2. Cluster 2 likely originates from the attempts of the algorithm to explore more regions to prevent confinement in the perceived minima.

From Figure 6c, the y-axis indicates the variable name and in descending order of importance for the contribution to the ML model used and the x-axis showing SHAP (Shapley additive explanations) value indicates the change in log-odds. The gradient color indicates the feature value yellow being high and blue being low. Each point presented in the rows originates from the original dataset. For instance, Na_2MoO_4 has one of the highest impacts on the ML model indicating that a high value has a negative impact on the goal. Curiously, it appeared that each of the components listed has a "sweet spot" to offer a positive impact on the goal. Multifaceted interaction between each component is reflected in the plot as there is no clear distinction between the contribution of each reagent except for H_2SO_4. This is consistent with the interaction and formation of POMs in the solution phase as the highly complex self-assembly process has yet to be fully understood.[39,40]

Results show that the algorithm-generated experiments allowed the platform to discover 18 variations which increased the CV area compared to the best combination from the

training data. The most promising samples, one of which increased the CV area by 45%, were taken forward as candidates for electrode material. The compositions were deposited on a GCE electrode using drop-casting method (Figure S34) and then the specific capacitance was measured (Figure S35–S36).Also, samples 1,2,6 and 7 of the deposited materials appeared to have pseudo-capacitance contributions like that of POM-deposited supercapacitor electrodes (see SI Section 3.10 for further details).[41–44]

Conclusions

In this work, we have shown a modular self-driving platform controlled by χDL for the efficient screening of complex redox systems coupled with ML. The work presented here shows how an inexpensive modular robotic platform has been reconfigured for use with vastly different chemistry. ECARUS performed over 16,300 operations over 480 hours without requiring servicing or replacements (Figure S37), proving the sturdiness of the platform. The electrochemical characterisation of the platform has been robustly tested using $(K_3/K_4)[Fe(CN)_6]$, showing the reference electrode is consistently well maintained throughout the experimental procedure. In addition, the initial tests have shown the gold working electrode is thoroughly cleaned after each sample, allowing for reliable analysis.

We showcased a system which can synthesise a range of inorganic complexes and conduct a traditional grid-search approach for the investigation of metal and ligand binding to explore a given chemical space. The exploration was able to explore 226 experiments in 280 hours during which ECARUS dispensed 2.3 L of reagents (Figure S37) and synthesised complexes which have considerably different CVs. The work showcased here highlights how ECARUS can save over a month of manual work and the results could be reliably repeated for further off-line analysis.

The platform has also been utilised to explore the role of acid type and concentration on the resultant pH and electrochemical behaviour of POM precursors. And was then coupled with an optimisation algorithm in the decision-making process for the closed-loop optimisation approach. Each of the synthetic conditions and characterisation of the closed-loop experiments were encoded with their standardised digital signature derived from χDL to ensure the reproducibility of the iterative experiments. Though naïve, the simplistic single-objective Bayesian optimisation algorithm showed signs of optimisation towards the set objective (maximum CV area) based on the robotic experiments.

This approach is an example of the materials acceleration platform (MAP) approach with a design-make-test-analyse (DMTA) cycle that could accelerate the search for desired redox properties in a redox-active system. The current limitation of the platform lies with the simplistic synthetic procedures by varying the composition of the reagents, pH adjustment, heating and stirring operations. Additional automated modules such as the vial-handling system, and filtration system in the robotic system would dramatically enhance the functionality of the system and enable more complex chemistry and material development. However, the modular nature of this automated electrochemistry platform proposes that it can be integrated into any other automated system which could resolve the limitation mentioned above. We believe that by providing a simplistic standardised modular open-sourced platform, researchers around the world could adopt such a system to accelerate the discovery of new materials in the coming future.

Experimental

General synthetic protocol used by ECARUS to synthesise cobalt and manganese coordination complexes: to each vial, ligands **1**–**6** (0–5 mL, in ethanol) were added with stirring. Followed by ethanol to make the volume up to 5 mL. Water (2 mL) was then added, followed by simultaneous addition of cobalt(II) chloride (1–2 mL, dissolved in water) and manganese(II) perchlorate (0–1 mL, dissolved in water). The solutions, with a final volume of 9 mL, were stirred to ensure complete mixing of the reagents. All solutions were then capped and heated to 60 °C overnight with stirring. The samples were allowed to cool before further analysis was carried out. Water (1 mL) or KCl (1 mL, 1 M stock in water when supporting electrolyte required) was added and the samples analysed by cyclic voltammetry or UV-Vis spectroscopy.

General protocol used by ECARUS for POM investigations: the platform dispensed the necessary reagents (in mL) into the vial based on the inputs. Stirring operation initiates, pH of the mixture is measured and pH is adjusted if required. The mixtures are stirred for 24 h at room temperature, then stirring operation is halted after allotted time and the CV experiments are carried out. Upon completion of the experiment, area of the CV is calculated using trapezoid rule. The composition of the reagents dispensed and calculated area is fed into the Bayesian optimisation algorithm and the following experiments were suggested by the algorithm and the cycle repeats. Electrodes are rinsed and electrochemically cleaned before being stored in KCl (3 M) solution when not in use.

Supporting Information

The Supplementary Information contains full information about how the platform was built, including the code used, information about all the experiments performed, and the relevant data produced. The authors have cited additional references within the Supporting Information (Ref. [45]).

Acknowledgements

This work was supported by LCs EPSRC grants (Grants EP/J015156/1; EP/L023652/1; EP/I033459/1; EP/J015156/1; EP/K023004/1; EP/L023652/1) and the ERC Advanced Grant (ERC-ADG, 670467 SMART-POM). Dr. Daniel Salley and Dr. Graham Keenan for the initial development of the automated platform which was integrated into this project. Dr. Dario Cambiè for technical support and mentorship at the beginning of the project.

Conflict of Interests

The authors declare no conflict of interest.

Data Availability Statement

The data that support the findings of this study are available in the supplementary material of this article.

Keywords: Electrochemistry · Automation · Machine-learning · Closed-loop Synthesis · Inorganic Chemistry

[1] R. D. Little, K. D. Moeller, *Chem. Rev.* **2018**, *118*, 4483–4484.
[2] Q. Sang, S. Hao, J. Han, Y. Ding, *EnergyChem* **2022**, *4*, 100069.
[3] G. E. Fryxell, S. V. Mattigod, Y. Lin, H. Wu, S. Fiskum, K. Parker, F. Zheng, W. Yantasee, T. S. Zemanian, R. S. Addleman, J. Liu, K. Kemner, S. Kelly, X. Feng, *J. Mater. Chem.* **2007**, *17*, 2863–2874.
[4] M. Yu, F. Liu, J. Li, J. Liu, Y. Zhang, F. Cheng, *Adv. Energy Mater.* **2022**, *12*, 2100640.
[5] S. Noreen, M. B. Tahir, A. Hussain, T. Nawaz, J. U. Rehman, A. Dahshan, M. Alzaid, H. Alrobei, *Int. J. Hydrogen Energy* **2022**, *47*, 1371–1389.
[6] X. Xu, S. Zhang, H. Chen, J. Kong, *Talanta* **2009**, *80*, 8–18.
[7] L. Barros, L. Cabrita, M. V. Boas, A. M. Carvalho, I. C. F. R. Ferreira, *Food Chem.* **2011**, *127*, 1600–1608.
[8] Y. Dai, W. Xu, R. A. Somoza, J. F. Welter, A. I. Caplan, C. C. Liu, *Angew. Chem. Int. Ed.* **2020**, *132*, 20726–20732.
[9] H. Chen, E. Kätelhön, R. G. Compton, *Curr. Opin. Electrochem.* **2023**, *38*, 101214.
[10] A. Mistry, A. A. Franco, S. J. Cooper, S. A. Roberts, V. Viswanathan, *ACS Energy Lett.* **2021**, *6*, 1422–1431.
[11] A. M. Bond, J. Zhang, L. Gundry, G. F. Kennedy, *Curr. Opin. Electrochem.* **2022**, *34*, 101009.
[12] L. Gundry, S.-X. Guo, G. Kennedy, J. Keith, M. Robinson, D. Gavaghan, A. M. Bond, J. Zhang, *Chem. Commun.* **2021**, *57*, 1855–1870.
[13] P. Puthongkham, S. Wirojsaengthong, A. Suea-Ngam, *Analyst* **2021**, *146*, 6351–6364.
[14] A. Dave, J. Mitchell, S. Burke, H. Lin, J. Whitacre, V. Viswanathan, *Nat. Commun.* **2022**, *13*, 5454.
[15] S. Steiner, J. Wolf, S. Glatzel, A. Andreou, J. M. Granda, G. Keenan, T. Hinkley, G. Aragon-Camarasa, P. J. Kitson, D. Angelone, L. Cronin, *Science* **2019**, *363*, eaav2211.
[16] A.-C. Bédard, A. Adamo, K. C. Aroh, M. G. Russell, A. A. Bedermann, J. Torosian, B. Yue, K. F. Jensen, T. F. Jamison, *Science* **2018**, *361*, 1220–1225.
[17] M. A. Soldatov, V. V. Butova, D. Pashkov, M. A. Butakova, P. V. Medvedev, A. V. Chernov, A. V. Soldatov, *Nanomaterials* **2021**, *11*, 619.
[18] C. W. Coley, D. A. Thomas, J. A. M. Lummiss, J. N. Jaworski, C. P. Breen, V. Schultz, T. Hart, J. S. Fishman, L. Rogers, H. Gao, R. W. Hicklin, P. P. Plehiers, J. Byington, J. S. Piotti, W. H. Green, A. J. Hart, T. F. Jamison, K. F. Jensen, *Science* **2019**, *365*, eaax1566.
[19] I. W. Davies, *Nature* **2019**, *570*, 175–181.
[20] T. Hardwick, N. Ahmed, *Chem. Sci.* **2020**, *11*, 11973–11988.
[21] J. M. Granda, L. Donina, V. Dragone, D.-L. Long, L. Cronin, *Nature* **2018**, *559*, 377–381.
[22] J. Bai, L. Cao, S. Mosbach, J. Akroyd, A. A. Lapkin, M. Kraft, *JACS Au* **2022**, *2*, 292–309.
[23] B. B. K., T. Pokhrel, D. Shrestha, A. Adhikari, B. Shirinfar, N. Ahmed, in *Encyclopedia of Solid-Liquid Interfaces (First Edition)* (Eds.: K. Wandelt, G. Bussetti), Elsevier, Oxford **2024**, pp. 23–35.
[24] D. M. Heard, A. J. J. Lennox, *Angew. Chem. Int. Ed.* **2020**, *59*, 18866–18884.
[25] M. R. Horn, A. Singh, S. Alomari, S. Goberna-Ferrón, R. Benages-Vilau, N. Chodankar, N. Motta, K. (Ken) Ostrikov, J. MacLeod, P. Sonar, P. Gomez-Romero, D. Dubal, *Energy Environ. Sci.* **2021**, *14*, 1652–1700.
[26] D. E. Katsoulis, *Chem. Rev.* **1998**, *98*, 359–388.
[27] K. D. Mjos, C. Orvig, *Chem. Rev.* **2014**, *114*, 4540–4563.
[28] D. S. Salley, G. A. Keenan, D.-L. Long, N. L. Bell, L. Cronin, *ACS Cent. Sci.* **2020**, *6*, 1587–1593.
[29] T. Minato, D. Salley, N. Mizuno, K. Yamaguchi, L. Cronin, K. Suzuki, *J. Am. Chem. Soc.* **2021**, *143*, 12809–12816.
[30] J. A. Hopkins Leseberg, W. C. Henke, J. D. Blakemore, in *Compr. Organomet. Chem. IV*, (Eds.: G. Parkin, K. Meyer, D. O'hare), Elsevier, Oxford **2022**, pp. 249–283.
[31] L. Porwol, D. J. Kowalski, A. Henson, D. Long, N. L. Bell, L. Cronin, *Angew. Chem. Int. Ed.* **2020**, *132*, 11352–11357.
[32] D. J. Kowalski, C. M. MacGregor, D.-L. Long, N. L. Bell, L. Cronin, *J. Am. Chem. Soc.* **2023**, *145*, 2332–2341.
[33] P. V. Bernhardt, G. A. Lawrance, in *Compr. Coord. Chem. II*, Elsevier **2003**, pp. 1–145.
[34] B. Bujanovic, S. Ralph, R. Reiner, K. Hirth, R. Atalla, *Materials* **2010**, *3*, 1888–1903.
[35] R. H. Atalla, L. A. Weinstock, R. S. Reiner, C. J. Houtman, S. Reichel, C. G. Hill, C. L. Hill, *Int. Symp. Wood Pulping Chem., 10th Atlanta,GA:* TAPPI Press **1999**, 408–412.
[36] A. Yu. Bychkov, V. V. Zujkov, *Dokl. Akad. Nauk - Rossijskaya Akademiya Nauk* **2005**, *400*, 69–71.
[37] S. Zhang, M. Han, *RSC Adv.* **2019**, *9*, 41720–41728.
[38] X. Liu, J. Cheng, M. Sprik, X. Lu, *J. Phys. Chem. Lett.* **2013**, *4*, 2926–2930.
[39] H. N. Miras, C. Mathis, W. Xuan, D.-L. Long, R. Pow, L. Cronin, *Proc. Natl. Acad. Sci. USA* **2020**, *117*, 10699–10705.
[40] R. Van Eldik, L. Cronin in *Adv. Inorg. Chem.*, (Eds., R. van Eldik, L. Cronin), Oxford, Elsevier **2017**, pp. 1–28.
[41] D. Cheng, B. Li, S. Sun, L.-J. Zhu, Y. Li, X.-L. Wu, H.-Y. Zang, *CCS Chem.* **2021**, *3*, 1649–1658.
[42] J. Suárez-Guevara, V. Ruiz, P. Gomez-Romero, *J. Mater. Chem. A* **2014**, *2*, 1014–1021.
[43] Y. Chen, M. Han, Y. Tang, J. Bao, S. Li, Y. Lan, Z. Dai, *Chem. Commun.* **2015**, *51*, 12377–12380.
[44] V. Ruiz, J. Suárez-Guevara, P. Gomez-Romero, *Electrochem. Commun.* **2012**, *24*, 35–38.
[45] T. Head, M. Kumar, H. Nahrstaedt, G. Louppe, I. Shcherbatyi (2021), scikit-optimize/scikit-optimize (v0.9.0). Zenodo. https://doi.org/10.5281/zenodo.5565057.

Manuscript received: October 5, 2023
Revised manuscript received: October 23, 2023
Version of record online: November 16, 2023